This is an accepted manuscript of an article published by Taylor & Francis Group in *International Journal of Remote Sensing* on April 24, 2016. Subject to 12 months' embargo period, embargo end date: April 24, 2017.

The version of record, Young Min Noh, Sung-Kyun Shin, Kwonho Lee, Detlef Müller & Kwanchul Kim (2016) “Utilization of the depolarization ratio derived by AERONET Sun/sky radiometer data for type confirmation of a mixed aerosol plume over East Asia”, *International Journal of Remote Sensing*, 37(10): 2008-2025, is available on line at DOI: 10.1080/01431161.2016.1176274

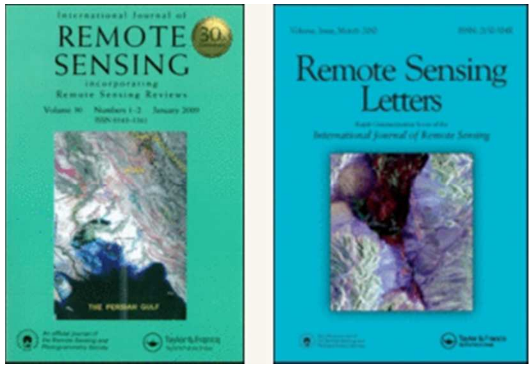

Utilization of Depolarization Ratio derived by AERONET Sun/Sky Radiometer Data for Type Confirmation of a Mixed Aerosol Plume over East Asia

Journal:	*International Journal of Remote Sensing*
Manuscript ID	TRES-PAP-2015-0873.R2
Manuscript Type:	IJRS Research Paper
Date Submitted by the Author:	n/a
Complete List of Authors:	Noh, Youngmin; Gwangju Institute of Science & Technology (GIST), International Environmental Research Center Shin, Sung-Kyun; Gangneung-Wonju National University, Department of Atmospheric and Environmental Sciences Lee, Kwonho ; Gangneung-Wonju National University, Department of Atmospheric and Environmental Sciences Mueller, Detlef; University of Hertfordshire, School of Physics, Astronomy and Mathematics Kim, Kwanchul; Gwangju Institute of Science & Technology (GIST), School of Environmental Science and Engineering
Keywords:	aerosols, lidar
Keywords (user defined):	depolarization ratio, sun/sky radiometer, size distribution

SCHOLARONE™
Manuscripts

Utilization of Depolarization Ratio derived by AERONET Sun/Sky Radiometer Data for Type Confirmation of a Mixed Aerosol Plume over East Asia

Young Min Noh[1], Sung-Kyun Shin[2], Kwonho Lee[3], Detlef Müller[4], and Kwanchul Kim[2*]

[1]*International Environmental Research Center, Gwangju Institute of Science & Technology (GIST), Korea*

[2]*School of Environmental Science and Engineering, Gwangju Institute of Science & Technology (GIST), Korea*

[3]*Department of Atmospheric and Environmental Sciences, Gangneung-Wonju National University, Korea*

[4]*School of Physics, Astronomy and Mathematics, University of Hertfordshire, Hertfordshire, UK*

[*]Corresponding Author

Kwanchul Kim

Tel.: +82-62-715-2830

Fax: +82-62-715-3404

Email: fehouse@gmail.com

For Peer Review Only

ABSTRACT

This paper confirms utilization of depolarization ratio derived by Ground-based Aerosol Robotics Network (AERONET) sun/sky radiometer data obtained during a high-PM_{10} episode at Gwangju, Korea (35.10°N, 126.53°E) in April 2009, in order to determine the nature and source of the atmospheric aerosol associated with this event. Integrated monitoring using satellite and depolarization lidar data, together with model analysis, was also completed for the period of the high-PM_{10} event. The sun/sky radiometer-derived particle depolarization ratio values are similar to the lidar-derived values, and these values highlight the effect of dust particles on aerosol observation. High particle depolarization ratios (12.5 - 14.2 %) were shown when the aerosol plume transported from the west between April 5 and 7. In contrast, lower particle depolarization ratios (5.8 - 9.8 %) were detected when the aerosol plume was transported from north in other observation days. Different optical properties are also shown according to variation of depolarization ratio. High values in the real part of the refractive index (1.47 - 1.49 at 440 nm), lower values in the imaginary part of the refractive index (0.007 - 0.009 at 440 nm), and a high proportion of coarser particles were observed during high depolarization ratio period. In contrast, the atmospheric aerosol transported from the north showed characteristics more commonly associated with smoke, with lower values in the real part of the refractive index (1.41 - 1.48 at 440 nm), higher values in the imaginary part of the refractive index (0.008 - 0.011), and a high proportion of fine particles. This indicates that the sun/sky radiometer-derived depolarization ratio is a useful parameter when estimating the effect of dust particles during high-PM_{10} events.

Key words: aerosols, lidar, depolarization ratio, sun/sky radiometer, size distribution

For Peer Review Only

1. Introduction

East Asia is one of the main global sources of atmospheric aerosol. This aerosol consists of anthropogenic aerosols originating from urban/industrial areas and natural aerosol such as dust from desert regions of central Asia, as well as smoke from forest fires in Siberia and agricultural burning (Murayama et al., 2004; Lee et al., 2005; Noh et al., 2011). Such aerosols have been studied previously within the context of their radiative effects and uncertain influences on climate forcing (Stocker et al., 2013). The importance of these aerosols to climate change is expected to increase in the future (Takemura et al., 2005). There are main types of atmospheric aerosols: (i) urban–industrial aerosol derived from fossil fuel combustion in populated industrial regions; (ii) biomass burning aerosol produced by forest and grassland fires; (iii) desert dust blown into the atmosphere by wind; and (iv) aerosol of marine origin (Dubovik et al., 2002). The significant differences in the optical properties of these main general aerosol types have been extensively studied (Dubovik et al., 2002; Eck et al., 2005; Russel et al., 2010; Utry et al., 2014). Eck et al. (2010) and Giles et al. (2012) have been studied about the mixture of dust and pollution particles mainly forcing on the variation of single-scattering albedo. However, there has been little analysis of mixed aerosol types, especially in Asian dust mixed cases in East Asia. Dust particles show definitely different optical properties with other aerosols (Dubovik et al., 2002; Russel et al., 2010; Hess et al., 1998).

South Korea is located in the downwind area from China in East Asia and is therefore an important region for observations of atmospheric aerosols; e.g., dust, smoke, and anthropogenic aerosols transported by westerly winds (Noh et al., 2008, 2009, 2011). Moreover, the different types of atmospheric aerosol generated in the individual source regions usually flow into Korea simultaneously (Noh et al., 2014). Thus, the observation of

For Peer Review Only

atmospheric aerosols in Korea requires further investigation, as the inflow of aerosol from multiple sources makes the determination and identification of aerosol properties a challenging task. To date, a large number of surface sampling measurements have been conducted to investigate atmospheric aerosol properties in Korea (Kim et al., 2008; Lasserre et al., 2008; Moon et al., 2008; Sahu et al., 2009; Jung et al., 2011). These surface sampling measurements, although frequently providing excellent data regarding aerosol mass concentrations and their chemical/physical properties, have been limited to ground concentrations, and it remains difficult to generate real-time data from such measurements.

In contrast, ground-based remote sensing of aerosol using wide angular and spectral measurements of solar and sky radiation are well-suited for detailed, reliable, and continuous monitoring of aerosol optical properties (Dubovik et al., 2002). Although ground-based aerosol remote sensing is widely used to monitor main aerosol, easy and specific method is not applied to quantitative analysis of mixed aerosol plumes until now.

The main purpose of this study is verifying the usefulness of the depolarization ratio derived by Ground-based Aerosol Robotics Network (AERONET) sun/sky radiometer data for the type classification of mixed aerosols. The data by satellite and depolarization lidar system is investigated to understand the transportation and distribution of atmospheric aerosols. The Hybrid Single Particle Lagrangian Integrated Trajectories (HYSPLIT) model and reanalysis data from the Monitoring Atmospheric Composition and Climate (MACC) model were also used to supplement the classification and identification of the origin of atmospheric aerosols. The remainder of this paper is organized as follows. Section 2 describes the monitoring site and measurement instruments used in this study. Section 3 presents the procedures used to classify the aerosol and describes the optical properties of aerosol transported to Korea, using the results obtained from the integrated monitoring of

For Peer Review Only

atmospheric aerosols. Finally, we discuss our results and the values for aerosol type classification in this study in Section 3.

2. Measurements

High PM_{10} levels (> 100 μg m^{-3}) were observed in Gwangju, South Korea between April 5 and 12 2009. Integrated monitoring of atmospheric aerosols was performed using the AERONET sun/sky radiometer and depolarization lidar at the Gwangju Institute of Science and Technology (GIST), Gwangju (35.10°N, 126.53°E), and using the Moderate Resolution Imaging Spectroradiometer (MODIS) on board the Terra and Aqua satellites.

2.1 Sun/sky radiometer

The AERONET sun/sky radiometer was operated at GIST. Column-integrated spectrally resolved aerosol measurements and sky-bright observations (almucantar measurements) were performed with the polarized-version of the CIMEL 381-1 automatic tacking sun/sky radiometer (Holben et al., 1998). The sun/sky radiometer measurements incorporated the radiances from four spectral channels at wavelengths of 440, 675, 870, and 1020 nm. Direct sun radiation at 15-minute intervals and sky radiation at 1-hour intervals were also observed. The sun/sky radiometer measurements were used to retrieve $\boldsymbol{\tau}$, the absorption Ångström exponents (AAE), the complex refractive index, and the size distribution via the AERONET algorithm. The Ångström exponents (AE) were retrieved directly from the optical depth measurements. Detailed information on the cloud-screening and inversion data retrieval algorithm can be found in Dubovik and King (2000). In the present study, we used

For Peer Review Only

AERONET level 2.0 data (quality assured), which can be downloaded from the AERONET website (http://aeronet.gsfc.nasa.gov).

The linear particle depolarization ratios strongly depend on particle shape. We calculated the depolarization ratio from the sun/sky radiometer data using the kernel look-up tables as described by Dubovik et al. (2006). Linear particle depolarization ratios ($\boldsymbol{\delta_{sp}}$) at the four wavelengths (440, 675, 870, and 1020 nm) were derived from the sun/sky radiometer measurements to identify non-sphericity within the observed aerosol. Detailed retrieval method is described by Lee et al. (2010c) as follows.

The elements $F_{11}(\lambda)$ and $F_{22}(\lambda)$ of the so-called Müller scattering matrices (Bohren et al., 1983) are computed from the retrieved complex refractive index and particle size distributions. The two parameters strongly depend on the angular and spectral distribution of the radiative intensity, which is measured with the AEROENT instrument (Dubovik et al., 2006). For unpolarized incident light, $F_{11}(\lambda)$ is proportional to the flux of the scattered light (Volten et al., 2001). Another input parameter that is needed for the retrieval of the linear particle depolarization ratio is the so-called aspect ratio distribution. The aspect ratio indicates the ratio of particle's longest axis to its shortest axis. In case of prolate particles, its polar diameter is greater than the equatorial diameter in contrast to oblate particles. The aspect ratio distribution is kept to a fixed distribution in the AERONET model, since scattering elements are nearly equivalent for all spheroid mixtures (Dubovik et al., 2006).

From the ratio of the elements $F_{11}(\lambda)$ and $F_{22}(\lambda)$ at the scattering angle $180°$ the linear particle depolarization ratio $\delta_p(\lambda)$ can be computed as (Dubovik et al., 2006)

$$\delta_p(\lambda) = \frac{1 - F_{22}(\lambda, 180°)/F_{11}(\lambda, 180°)}{1 + F_{22}(\lambda, 180°)/F_{11}(\lambda, 180°)} \times 100(\%) \tag{1}$$

For Peer Review Only

2.2 Depolarization lidar

The depolarization lidar system was used to monitor the vertical distribution of observed aerosols during the high-PM_{10} levels. Measurements with the GIST multiwavelength Raman LIDAR system were carried out at the same site as that of the AERONET sun/sky radiometer. For a detailed description of the multiwavelength aerosol lidar system, the methodology used to analyze the optical data, and uncertainty analysis, see Noh et al. (2007, 2008, 2009). The vertical distribution of observed aerosols can be obtained using the aerosol backscatter coefficient. The parallel- and perpendicular-polarized signal components (with respect to the plane of polarization of the emitted laser beam) were measured at 532 nm to derive the aerosol backscatter coefficient and the linear volume depolarization ratio ($\boldsymbol{\delta}$). The linear particle depolarization ratio ($\boldsymbol{\delta_p}$) differs from $\boldsymbol{\delta}$ as it depends on the concentration of particles in relation to the concentration of air molecules. $\boldsymbol{\delta_p}$ is calculated as an intensive parameter and can be used to qualitatively describe the average morphology of the measured aerosol particles. We applied the equation to retrieve the $\boldsymbol{\delta_p}$, as proposed by Noh et al. (2013). The value of $\boldsymbol{\delta_p}$ is 0 % for an ideal spherical particle. In the presence of dust particles, the depolarization ratio increases up to 30 %, depending on the amount of dust particles in the aerosol plume (Shimizu et al., 2004; Noh et al., 2012, 2014; Shin et al., 2014).

The PM_{10} concentrations were measured at the Gwangju Local Meteorological Administration building, 5 km from the observation site.

2.3 Satellite data

Satellite observations such as AVHRR, SeaWIFS, MODIS, MISR, and GOCI have previously been used to monitor air quality and estimate the location and extent of aerosols

For Peer Review Only

(Rao et al., 1989; Gordon and Wang, 1994; Kaufman et al., 1997; Lee et al., 2010a). A dataset collected by MODIS was used during a period when it was performing the integrated monitoring of atmospheric aerosol. The spatial distribution of Aerosol Optical Depth (AOD ($\boldsymbol{\tau}$)) at 550 nm from MODIS and the MODIS SaTellite Aerosol Retrieval (MSTAR) algorithm, as reported by Lee et al. (2010b), were used to determine the origin and track the long-range transport of atmospheric aerosol.

2.4 Model simulations for Backward Trajectories and Pollution emission

The Hybrid Single Particle Lagrangian Integrated Trajectory (HYSPLIT) model (Draxler and Rolph, 2003) was used to generate 5-day backward trajectories for air masses arriving over the measurement site at the altitude of the aerosol layers observed by the depolarization lidar. These trajectories allowed us to track the origin of the aerosol layers and their transport pathway. The European Centre for Medium-range Weather Forecast (ECMWF) provides aerosol reanalysis data as part of the MACC project. These data assimilate the satellite data (e.g., the AOD ($\boldsymbol{\tau}$) retrieved by MODIS) into the global model. Thus, the reanalysis data are considered as comparably reliable data because corrections for the model departure from observational data were performed during the assimilation (Bellouin et al., 2013). This reanalysis provides information on pollution caused by the emission of various aerosols, as well as chemically reactive gases and greenhouse gases. We used the $\boldsymbol{\tau}$ values of dust particles, black carbon, and organic matter from the MACC reanalysis data to determine the intensity of pollution along the transport pathway and to estimate the characteristics of atmospheric aerosols.

For Peer Review Only

3. Results

3.1 High-PM_{10} episode, April 9–12 2009

Hourly averaged surface PM_{10} concentrations were obtained using a beta gauge between 00:00 local time (LT) April 5 and 24:00 LT on April 12 are plotted in Fig. 1. The PM_{10} concentration begins to increase above the South Korea's 24-hour PM_{10} standard (100 μg m^{-3}) from April 5 (15:00 LT), and these high values were continuously observed until April 12 (12:00 LT). The PM_{10} concentrations only fell below this level on April 7 (15:00 - 21:00 LT) and April 9 (14:00 - 17:00 LT).

The values of $\boldsymbol{\tau_{500}}$ (AOD at 500 nm), AE at 440 - 870 nm, and AAE at 440 - 870 nm measured with the AERONET sun/sky radiometer and $\boldsymbol{\tau_{550}}$ (AOD at 550 nm) retrieved by MODIS are shown in Fig. 1 and Table 1. The temporal variations in $\boldsymbol{\tau_{500}}$ and $\boldsymbol{\tau_{550}}$ are similar to those of PM_{10} levels. Values of $\boldsymbol{\tau_{500}}$ and $\boldsymbol{\tau_{550}}$ increased when the PM_{10} concentration increased, whereas the lower values of $\boldsymbol{\tau_{500}}$ and $\boldsymbol{\tau_{550}}$ were measured as the concentration decreased in most cases. Differences in the values of the AEs were recorded during the high-PM_{10} episode. The AE values measured during April 6 - 8 2009 were in the range 1.24 - 1.38 (average = 1.31 ± 0.06), and thus considerably lower than those recorded during April 9 - 11 2009 (1.42 - 1.53, average = 1.47 ± 0.04). These differences suggest that the aerosol layers observed from April 5 to 8 contained a higher concentration of large aerosol particles when compared with the average particle size in the aerosol layer observed from April 9 to 11. This result is possibly related to differences in the types and sources of the atmospheric aerosols.

The AAEs measured during April 6 - 8 2009 were in the range 0.62 - 1.36 (average = 1.03 ± 0.20) and thus were similar to those recorded during April 9 - 11 2009 (0.85 - 1.59, average = 1.06 ± 0.21). Russell et al. (2010) showed that AAE is correlated with aerosol

For Peer Review Only

composition or type, and reported AAE values near 1 for AERONET-measured aerosol columns dominated by urban–industrial aerosol. Although the aerosol size was different between the two periods, as inferred from AE values, the main aerosol type using the AAE can be estimated. However, a more detailed analysis is required to determine which atmospheric aerosol types caused the high PM_{10} levels during early April of 2009.

Figure 2 shows time–height cross-sections of the aerosol backscatter coefficient and the volume depolarization ratio (**δ**) derived from continuous depolarization ratio lidar measurements between April 5 and 12 2009. No observations were made from 12:00 LT on April 8 to 00:00 LT on April 9 because of precipitation. Figure 2(a) shows the presence of atmospheric aerosol that was detected mostly within the planetary boundary layer (1 - 2 km altitude) during the observation periods. The significant atmospheric aerosol layers were defined using their relatively high backscatter coefficients at low altitudes. However, the backscatter coefficients shown in Fig. 2(a) only provide qualitative information and the vertical distribution of atmospheric aerosol. A preliminary classification of the types of atmospheric aerosol observed during this period was made using the **δ** values shown in Fig. 2(b). **δ** is a reliable indicator of particle shape and can be used to distinguish between non-spherical and spherical particles (Shimizu et al., 2004, Noh et al., 2012, Shin et al., 2015). In Fig. 2(b), the **δ** values begin to increase in the layer between 1 and 2 km on April 5 2009. The values of **δ** greater than 10 % suggest the inflow of atmospheric aerosol containing dust particles. The higher **δ** values (ca. 13 %) detected from April 6 to 8 indicate that the atmospheric aerosol over Korea contained a higher amount of dust particles than on other observation days. In contrast, the **δ** value in the layer around 2 km decreased from April 9 onwards. This might point to the inflow of another type of atmospheric aerosol at higher altitudes, although atmospheric aerosols with relatively high depolarization ratios (> 8 %)

For Peer Review Only

were still detected at lower altitudes.

3.2 Classification of aerosol source

Figure 3 shows the results from the HYSPLIT backward trajectories and the distribution of **τ** at 550 nm for dust, black carbon, and organic matter obtained from the MACC model and calculated using ECMWF reanalysis data. The distribution of the aerosol optical depth derived from MODIS is also shown in Fig. 3.

The consistently high values of **τ** detected by MODIS correspond with the high aerosol loading for the observation period. The heights of the aerosol layers were determined from the lidar measurements; i.e., the aerosol layers with heights that correspond to increased backscatter coefficients and δ values, for the calculation of the HYSPLIT model. The HYSPLIT model shows different transport pathways and source regions of the aerosol layer observed on each measurement day. The air masses were transported to the observation site from either the west or northwest of the monitoring site (eastern and northeast China, respectively) over April 6 - 8, as shown in Fig. 3 (a1 - c1). In contrast, the backward trajectories for arrival heights of 1600 and 2000 m on April 9 differ from the air mass movement patterns for April 6 - 8. On April 9, the air masses that passed over the monitoring site at 1600 and 2000 m were more likely to have arrived from the north via North Korea, whereas the air masses at lower altitudes (800 and 1200 m) were transported from the west/northwest regions. The changes in the air mass movement patterns were more obvious on April 10 and 11. The air masses that arrived at the observation site at higher altitudes (1600 and 2000 m) on April 10 and 11 had passed over Siberia and North Korea. However, the air masses that passed over the observation site at lower altitudes on April 10 and 11 were

For Peer Review Only

transported from desert regions and passed over eastern and northeast China. The aerosols observed on April 12 seem to have been generated from local sources. We consider that the aerosol load during the high-PM_{10} episodes was caused by the transportation of various aerosols from different source regions.

The differing source regions and origins of each transported aerosol result in different aerosol compositions. Those air masses with a desert origin might consist primarily of dust particles, whereas those transported over densely populated/highly industrialized areas are likely to include anthropogenic pollutants. The smoke particles, possibly derived from biomass/forest burning in Siberia and North Korea, are more likely to contain black carbon and organic matter. The distribution of $\boldsymbol{\tau}$ for dust, black carbon, and organic matter computed by the MACC model using the ECMWF reanalysis data were used to estimate the distribution of the various aerosols transported to Korea, as shown Fig. 3 (a3 - g5). The dust particles emitted from the desert regions of Inner Mongolia were transported across China and affected Korea during April 7 - 9. The model values of $\boldsymbol{\tau}$ for the dust over Korea on April 7 - 9 are significantly higher than for the other dates during the monitoring period. The $\boldsymbol{\tau}$ of black carbon that possibly originated from industrial regions of China was also significantly higher on April 7 - 9. On the other hand, the $\boldsymbol{\tau}$ of black carbon and organic matter over Siberia and on the transport pathway of the air masses increased from April 9 onwards. Figure 4 shows the accumulated fire spots obtained from the MODIS thermal anomalies/fire product (Kaufman et al., 1998) for April 9 - 12 2009. Although a few fire spots were detected in northeast China, most were in northeast Siberia and North Korea. This suggests that aerosols observed on April 9 - 11 were affected by the transport of smoke from Siberia. As a result, the $\boldsymbol{\tau}$ of black carbon and organic matter in Siberia on these observation days increased. On the basis of the distribution of $\boldsymbol{\tau}$ for various aerosols obtained from the MACC model, and the

For Peer Review Only

transport pathway of aerosol retrieved from the HYSPLIT model, we conclude that the types of aerosol that generated the high-PM_{10} event were dust particles, anthropogenic pollutants, and smoke particles. Moreover, the influence of these aerosols on high aerosol loading over Korea varied according to the mass movement patterns of the atmosphere on each measurement day.

3.3 Depolarization ratio

Lidar-derived $\boldsymbol{\delta_p}$ values can be used to estimate the amount of mixed dust in aerosol plumes (Shimizu et al., 2004; Tesche et al., 2011; Noh et al., 2012; 2014). However, sun/sky radiometer-derived $\boldsymbol{\delta_{sp}}$ values have previously been applied only to the study of Saharan dust (Müller et al., 2010). Figure 5 shows $\boldsymbol{\delta_{sp}}$ values at four wavelengths derived from the sun/sky radiometer data, and the column-integrated $\boldsymbol{\delta_p}$ at 532 nm derived from the lidar system. The correlation of $\boldsymbol{\delta_p}$ between lidar and sun/sky radiometer is shown in Figure 6. The depolarization ratios from the two instruments are in relatively good agreement throughout the observation period. However, the $\boldsymbol{\delta_p}$ by lidar in many cases was lower than the AERONET sun/sky radiometer-derived $\boldsymbol{\delta_{sp}}$. The vertical distribution of $\boldsymbol{\delta}$ in Fig. 2 (b) shows that $\boldsymbol{\delta}$ decreases above an altitude of 0.5 km from April 12 (09:00 LT). However, we must remember that the lidar-derived data do not take account of the optical properties of the aerosols below 0.5 km. The incomplete overlap between the laser beam and the field of view of the receiver telescope does not allow for a reliable retrieval of lidar profiles in this altitude range (Noh et al., 2013). Considering the high $\boldsymbol{\delta_{sp}}$ and $\boldsymbol{\tau}$ values obtained from the sun/sky radiometer data, it seems that the dust particles inducing high $\boldsymbol{\delta}$ existed below the lidar overlap height.

For Peer Review Only

The value of δ_{sp} at 440 nm was greater than that at the other wavelengths in most cases. Müller et al. (2010) reported that the values increase with wavelength for the pure dust cases. However, δ_{sp} decreases with wavelength for mixed dust cases (Lee et al., 2010c). From these results, the aerosols in this study can be interpreted as mixed dust. However, the daily average values listed in Table 1 show clear differences over time. The δ_{sp} values at 440 nm between April 5 and 8 (12.5 - 14.2 %) were higher than them between April 9 and 11 (5.8 - 9.8 %). The depolarization ratios of individual aerosol types have been reported previously; e.g., 10 - 20 % for polluted dust (Shimizu et al., 2004; Tesche et al., 2011; Burton et al., 2012; Shin et al., 2013), 30 - 35 % for pure dust (Murayama et al., 2004; Freudenthaler et al., 2009), 4 - 9 % for smoke (Murayama et al., 2004), and < 5 % for pollution particles (Yoon et al., 2010). If we consider only daily average δ_{sp} values, the aerosol observed over the periods April 5 - 8 and 9 - 11 can be categorized as polluted dust and smoke particles, respectively. However, the data in Fig. 5 (e and f) show relatively high δ_{sp} values of 8.3 - 11.6 % in the morning on April 9 and 10. Lidar-derived δ_{p} also shows values that are 1 - 3 % higher in the morning than afternoon in Fig. 2 (b). The distribution of dust calculated using the MACC model (Fig. 3) shows that the dust particles are continuously distributed around South Korea. The relatively high values of δ_{sp} in the morning on April 9 and 10 is likely to have been caused by dust particles. The relatively high δ_{sp} values on April 12 are also likely to have been affected by dust particles.

3.4 Optical/microphysical properties

Figure 7 shows the daily average value of the real and imaginary parts of the refractive index at 440, 675, 875, and 1020 nm obtained from the AERONET sun/sky radiometer between April 5 and 12.

For Peer Review Only

The real part of the refractive index describes the scattering properties, whereas the imaginary part describes the absorption properties of the particles (Barber et al., 1999). Differences in the values of the refractive index were found for the different aerosol transport pathways on each measurement day. The values of the real part of the refractive index measured on April 7 and 8 were 1.47 ± 0.06 and 1.49 ± 0.03, respectively, at 440 nm. These values are larger, and less variable, than those measured between April 9 and 12, which were 1.41 ± 0.03 to 1.46 ± 0.04, 1.44 ± 0.03 to 1.47 ± 0.03, 1.45 ± 0.03 to 1.48 ± 0.02, and 1.45 ± 0.02 to 1.47 ± 0.02 at 440, 675, 870, and 1020 nm, respectively.

Several previous studies have reported the real part of the refractive index for various aerosols. For example, Dubovik et al. (2002) used AERONET sun/sky radiometer data and observed the real part of refractive index values of 1.55 ± 0.03 to 1.56 ± 0.03 for desert dust, of 1.47 and 1.52 for smoke derived from biomass burning in the Amazonian forest region and in the South American Cerrado, respectively, and lower values for urban/industrial aerosols. In this study the real part of refractive index values ranged from 1.39 to 1.47. Noh et al. (2009, 2011) reported values for smoke aerosols from Siberia and northern China, and urban haze from northeast China, of 1.41 ± 0.03 to 1.42 ± 0.02 and 1.44 ± 0.03 to 1.44 ± 0.05, respectively.

The value of the imaginary part of the refractive index, which represents the light-absorption properties of the aerosol particles, tended to vary according to the aerosol source region. Lower values for the imaginary part were measured on April 7 and 8 in the ranges 0.008 - 0.009, 0.008 - 0.007, 0.008 - 0.007, and 0.009 - 0.007 at 440, 675, 870, and 1020 nm, respectively. These values are higher than the values for the imaginary part of desert dust reported by Dubovik et al. (2002) of 0.0025 - 0.0029, 0.0013 - 0.0014, 0.001, and 0.001 at 440, 670, 870, and 1020 nm, respectively. The values of the imaginary part of the refractive

For Peer Review Only

index increased when the source and transport pathway of the aerosol changed, and were higher between April 9 and 11 (by about 0.01) than on April 7 and 8. These differences between the real and imaginary parts of the refractive index indicate that the aerosol types changed during the high-PM_{10} episode. However, it is difficult to classify the aerosol types using only the refractive index data obtained during the high-PM_{10} episode.

Figure 8 shows the particle volume size distributions observed at the same time as $\boldsymbol{\tau}$ in Fig. 1. The distribution is bimodal in all cases, but the dominant particle size changes over the monitoring period. A fine-mode dominance is evident on April 5, the size distribution on April 7 and 8 shows sub-equal amounts of fine and coarse particles, and finer material is again dominant during April 9 - 12. The presence of larger particles on April 7 and 8 suggests that dust particles were transported into the region on these days. A significant fine fraction (< 0.5 μm) is also apparent in the size distribution, which we interpret to indicate that the aerosol particles transported on April 7 and 8 were a mixture of dust and anthropogenic particles. However, the proportion of fine particles increased from April 9 onwards. The proportion of finer particles was much greater on April 10 and 11 (Fig. 8), possibly related to the dominance of smoke particles that originated from Siberia and North Korea, as explained previously.

Figure 9 shows daily averaged single scattering albedo (SSA) at four wavelengths (440, 675, 870, and 1020 nm) from 5 to 12 April 2009. The spectral SSA behavior can be utilized for main aerosol type classification (Dubovik et al., 2002; Eck et al., 2005; 2010; Giles et al., 2012). Increasing spectral SSA behavior is observed for dust particle. In contrast, urban/industrial or biomass burning aerosol shows the decreasing spectral SSA behavior (Eck et al., 2005). In mixed cases, these spectral behaviors are lessened (Eck et al., 2005; 2010; Giles et al., 2012). Since the mixed plume of dust and anthropogenic/biomass burning

For Peer Review Only

particles was observed during research period, clear pattern of spectral SSA behavior for aerosol type classification was not shown in Figure 9. However, Increase of SSA between 440 and 675 nm was shown on 7 and 8 April 2009 at the dust dominant cases. Spectral SSA behavior of anthropogenic/biomass burning particle was observed on 6 April 2009 even though bimodal size distribution is detected. Those results denote that the spectral SSA behavior also needs support of other parameters to clearly classify aerosol type.

4. Summary and conclusions

In this study, satellite, lidar, and AERONET sun/sky radiometer data, in combination with data from the HYSPLIT and MACC models, were analyzed to determine the sources of observed atmospheric aerosol. We found that high PM_{10} levels were affected differently by dust, and anthropogenic and smoke aerosols.

The sun/sky radiometer-derived $\boldsymbol{\delta_{sp}}$ values are similar to the lidar-derived values, and these values highlight the effect of dust particles on aerosol observation, as the depolarization ratio is directly related to the non-sphericity of particles. From these values, we can infer that dust particles were continuously present during the high-PM_{10} episode, but were most prominent during April 5 - 8 based on the relatively elevated $\boldsymbol{\delta_{sp}}$ values of between 12.5 % and 14.2 %. And the aerosol plume transported from the west between at that time. In contrast, lower particle depolarization ratios (5.8 - 9.8 %) were detected when the aerosol plume was transported from north in other observation days.

The optical and microphysical properties of atmospheric aerosol retrieved from the AERONET sun/sky radiometer data during the high-PM_{10} episode showed similar trend with $\boldsymbol{\delta_{sp}}$ during observation period. The atmospheric aerosol transported from the west showed

For Peer Review Only

higher values in the real part of the refractive index, lower values in the imaginary part of the refractive index, and a high proportion of coarser particles. In contrast, the atmospheric aerosol transported from the north showed lower values in the real part of the refractive index, higher values in the imaginary part of the refractive index, and a greater proportion of finer particles. However, the use of these parameters alone is generally insufficient to clarify the effect of dust particles on the mixed aerosol plumes. We can clearly classify the aerosol type and the degree of mixing among various aerosols when depolarization ratio is analyzed with other optical and microphysical parameters.

If $\boldsymbol{\delta_{sp}}$ values are combined with other optical and microphysical parameters retrieved from AERONET sun/sky radiometer data, it is possible to estimate the aerosol characteristics and degree of mixing of dust particles without the support of other analytical techniques.

Acknowledgements

This work was funded by the Korea Meteorological Administration Research and Development Program under Grant KMIPA2015-6150. This research was also supported by the International Environmental Research Center (IERC)

References

Barber, and Thomas A., 1999: Control of particulate matter contamination in healthcare manufacturing. *1st ed., Englewood: Interpharm Press*, 363-408.

Bellouin, N., Quaas, J., Morcrette, J. J., and Boucher, O., 2013: Estimates of aerosol radiative

For Peer Review Only

forcing from the MACC re-analysis. *Atmospheric Chemistry and Physics*, **13(4)**, 2045-2062.

Bohren, C. F., & Huffman, D. R., 1983: Absorption and scattering of light by small particles. *Wiley*, New York, 541p.

Burton, S. P., Ferrare, R. A., Hostetler, C. A., Hair, J. W., Rogers, R. R., Obland, M. D., Butler, C. F., Cook, A. L., Harper D. B., and Froyd, K. D., 2012: Aerosol classification using airborne High Spectral Resolution Lidar measurements–methodology and examples. *Atmospheric Measurement Techniques*, **5(1)**, 73-98.

Draxler, R. R., and Rolph, G. D., 2003: HYSPLIT (HYbrid Single-Particle Lagrangian Integrated Trajectory) model access via NOAA ARL READY website (http://www. arl. noaa. gov/ready/hysplit4. html). NOAA Air Resources Laboratory, Silver Spring.

Dubovik, Oleg, and Michael D. King., 2000: A flexible inversion algorithm for retrieval of aerosol optical properties from Sun and sky radiance measurements. *Journal of Geophysical Research: Atmospheres (1984–2012)*, **105(D16)**, 20673-20696.

Dubovik, O., Holben, B., Eck, T. F., Smirnov, A., Kaufman, Y. J., King, M. D., Tanre D., and Slutsker, I., 2002: Variability of absorption and optical properties of key aerosol types observed in worldwide locations. *Journal of the atmospheric sciences*, **59(3)**, 590-608.

Dubovik, O., Sinyuk, A., Lapyonok, T., Sinyuk, A., Mishchenko, M. I., Yang, P., Eck, T. F., Volten, H., Munoz, O., Veihelmann, B., van der Zander, W. J., Sorokin, M., and Slutsker, I., 2006: Application of light scattering by spheroids for accounting for particle non-sphericity in remote sensing of desert dust. *J. Geophys. Res.*, **111**, D11208, doi:10.1029/2005JD006619.

For Peer Review Only

Eck, T. F., Holben, B. N., Dubovik, O., Smirnov, A., Goloub, P., Chen, H. B., Chatenet, B., Gomes, L., Zhang, X.-Y., Tsay, S.-C., Ji, Q., Giles, D., and Slutsker, I., 2005: Columnar aerosol optical properties at AERONET sites in central eastern Asia and aerosol transport to the tropical mid-Pacific. *J. Geophys. Res.*, **110**, D06202, doi:10.1029/2004JD005274.

Eck, T. F., Holben, B. N., Sinyuk, A., Pinker, R. T., Goloub, P., Chen, H., Chatenet, B., Li, Z., Singh, R. P., Tripathi, S. N., Reid, J. S., Giles, D. M., Dubovik, O., O'Neill, N. T., Smirnov, A., Wang, P., and Xia, X., 2010: Climatological aspects of the optical properties of fine/coarse mode aerosol mixtures, *J. Geophys. Res.*, **115**, D19205, doi:10.1029/2010JD014002.

Freudenthaler, V., Esselborn, M., Wiegner, M., Heese, B., Tesche, M., Ansmann, A., Müller, D., Althausen, D., Wirth, M., Fix, A., Ehret, G., Toledano, C., Garhammer, M., and Seefeldner, M., 2009: Depolarization ratio profiling at several wavelengths in pure Saharan dust during SAMUM 2006. *Tellus B*, **61(1)**, 165-179.

Giles, D. M., B. N. Holben, T. F. Eck, A. Sinyuk, A. Smirnov, I. Slutsker, R. R. Dickerson, A. M. Thompson, and J. S. Schafer, 2012: An analysis of AERONET aerosol absorption properties and classifications representative of aerosol source regions, *J. Geophys. Res.*, **117**, D17203, doi:10.1029/2012JD018127

Gordon, H. R. and Wang, M., 1994: Retrieval of water-leaving radiance and aerosol optical thickness over the oceans with Sea-WiFS: A preliminary algorithm. *Appl. Optics*, **33**, 443–452.

Hess, M., P. Koepke, and I. Schult, 1998: Optical properties of aerosols and clouds: The software package OPAC. Bull. Amer. Meteor. Soc., 79, 831–844.

For Peer Review Only

Holben, B.N., Eck, T.F., Slutsker, I., Tanre, D., Buis, J.P., Setzer, A., Vermote, E., Reagan, J.A., Kaufman, Y.J., Nakajima, T., Lavenu, F., Jankowiak, I., and Smirnov, A., 1998: AERONET - A federated instrument network and data archive for aerosol characterization. *Remote Sens. Environ.*, **66(1)**, 1-16.

Jung, J., and Kim, Y. J., 2011: Tracking sources of severe haze episodes and their physicochemical and hygroscopic properties under Asian continental outflow: Long-range transport pollution, postharvest biomass burning, and Asian dust. *Journal of Geophysical Research: Atmospheres (1984–2012)*, **116(D2)**.

Kaufman, Y. J., Wald, A. E., Remer, L. A., Gao, B. C., Li, R.-R., and Flynn, L., 1997: The MODIS 2.1-mm channel correlation with visible reflectance for use in remote sensing of aerosol. *IEEE T. Geosci. Remote*, **35**, 1286–1298.

Kaufman, Y. J., Justice, C. O., Flynn, L. P., Kendall, J. D., Prins, E. M., Giglio, L., Ward, D. E. Menzel W. P., and Setzer, A. W., 1998: Potential global fire monitoring from EOS-MODIS. *Journal of Geophysical Research: Atmospheres (1984–2012)*, **103(D24)**, 32215-32238.

Kim, K. W., Kim, Y. J., and Bang, S. Y., 2008: Summer time haze characteristics of the urban atmosphere of Gwangju and the rural atmosphere of Anmyon, Korea. *Environmental monitoring and assessment*, **141(1-3)**, 189-199.

Lasserre, F., Cautenet, G., Bouet, C., Dong, X., Kim, Y. J., Sugimoto, N., Matsui, I., and Shimizu, A., 2008: A model tool for assessing real-time mixing of mineral and anthropogenic pollutants in East Asia: a case study of April 2005. *Atmospheric Chemistry and Physics*, **8(13)**, 3603-3622.

For Peer Review Only

Lee, J., Kim, J., Song, C. H., Ryu, J. H., Ahn, Y. H., and Song, C. K., 2010a: Algorithm for retrieval of aerosol optical properties over the ocean from the Geostationary Ocean Color Imager. *Remote Sensing of Environment*, **114(5)**, 1077-1088.

Lee, K. H., and Y. J. Kim., 2010b: Satellite remote sensing of Asian aerosols: a case study of clean, polluted, and Asian dust storm days. *Atmospheric Measurement Techniques*, **3(6)**, 1771-1784.

Lee, K. H., Muller, D., Noh, Y. M., Shin, S. K., and Shin, D. H., 2010c: Depolarization ratio retrievals using AERONET sun photometer data. *Journal of the Optical Society of Korea*, **14(3)**, 178-184.

Lee, K. H., Kim, J. E., Kim, Y. J., Kim, J., and von Hoyningen-Huene, W., 2005: Impact of the smoke aerosol from Russian forest fires on the atmospheric environment over Korea during May 2003. *Atmospheric Environment*, **39(1)**, 85-99.

Moon, K. J., Han, J. S., Ghim, Y. S., and Kim, Y. J., 2008: Source apportionment of fine carbonaceous particles by positive matrix factorization at Gosan background site in East Asia. *Environment international*, **34(5)**, 654-664.

Murayama, T., Müller, D., Wada, K., Shimizu, A., Sekiguchi, M., and Tsukamoto, T., 2004: Characterization of Asian dust and Siberian smoke with multi-wavelength Raman lidar over Tokyo, Japan in spring 2003. *Geophysical Research Letters*, **31(23)**.

Müller, D., Ansmann, A., Freudenthaler, V., Kandler, K., Toledano, C., Hiebsch, Gasteiger, J., Esselborn, M., Tesche, M., Heese, B., Althausen, D., Weinzierl, B., Petzold, A., and von Hoyningen-Huene, W., 2010: Mineral dust observed with AERONET Sun photometer,

For Peer Review Only

Raman lidar, and in situ instruments during SAMUM 2006: Shape-dependent particle properties. *J. Geophys. Res*., **115**, D11207, doi:10.1029/2009JD012523.

Noh, Y. M., Kim, Y. J., Choi, B. C., and Murayama, T., 2007: Aerosol lidar ratio characteristics measured by a multi-wavelength Raman lidar system at Anmyeon Island. *Korea. Atmos. Res.,* **86**, 76–87.

Noh, Y. M., Kim, Y. J., and Müller, D. 2008: Seasonal characteristics of lidar ratios measured with a Raman lidar at Gwangju, Korea in spring and autumn. *Atmos. Environ.*, **42**, 2208–2224.

Noh, Y. M., Müller, D., Shin, D. H., Lee, H., Jung, J. S., Lee, K. H., Cribb, M., Li, Z., and Kim, Y. J., 2009: Optical and microphysical properties of severe haze and smoke aerosol measured by integrated remote sensing techniques in Gwangju, Korea. *Atmospheric Environment*, **43(4)**, 879-888.

Noh, Y. M., Müller, D., Mattis, I., Lee, H., and Kim, Y. J., 2011: Vertically resolved light-absorption characteristics and the influence of relative humidity on particle properties: Multiwavelength Raman lidar observations of East Asian aerosol types over Korea. *Journal of Geophysical Research*, **116**: D06206,doi: 10.1029/2010JD014873.

Noh, Y. M., Müller, D., Lee, H., Lee, K., Kim, K., Shin, S., and Kim, Y. J., 2012: Estimation of radiative forcing by the dust and non-dust content in mixed East Asian pollution plumes on the basis of depolarization ratios measured with lidar. *Atmospheric Environment*, **61**, 221-231.

Noh, Y. M., Lee, H., Mueller, D., Lee, K., Shin, D., Shin, S., Choi, T. J., Choi, Y. J., and Kim, K. R., 2013: Investigation of the diurnal pattern of the vertical distribution of pollen in the

For Peer Review Only

lower troposphere using LIDAR. *Atmospheric Chemistry and Physics*, **13(15)**, 7619-7629.

Noh, Y. M., 2014: Single-scattering albedo profiling of mixed Asian dust plumes with multiwavelength Raman lidar. *Atmospheric Environment*, **95**, 305-317.

Park, S. S., Kim, Y. J., Cho, S. Y., and Kim, S. J., 2007: Characterization of $PM_{2.5}$ aerosols dominated by local pollution and Asian dust observed at an urban site in Korea during aerosol characterization experiments (ACE)–Asia Project. *Journal of the Air & Waste Management Association*, **57(4)**, 434-443.

Rao, C. R. N., McClain, E. P., and Stowe, L. L., 1989: Remote sensing of aerosols over the oceans using AVHRR data theory, practice, and applications. *Int. J. Remote Sens.*, **10(4–5)**, 743–749.

Russell, P. B., Bergstrom, R. W., Shinozuka, Y., Clarke, A. D., DeCarlo, P. F., Jimenez, J. L., Redemann, J., Dubovik O., and Strawa, A., 2010: Absorption Angstrom Exponent in AERONET and related data as an indicator of aerosol composition. *Atmospheric Chemistry and Physics*, **10(3)**, 1155-1169.

Sahu, L. K., Kondo, Y., Miyazaki, Y., Kuwata, M., Koike, M., Takegawa, N., Tanimoto, H., Matsueda, H., Yoon, S. C., and Kim, Y. J., 2009: Anthropogenic aerosols observed in Asian continental outflow at Jeju Island, Korea, in spring 2005. *J. Geophys. Res.*, **114**, D03301, doi:10.1029/2008JD010306.

Shimizu, A., Sugimoto, N., Matsui, I., Arao, K., Uno, I., Murayama, T., Kagawa, N., Aoki, K., Uchiyama, A., and Yamazaki, A., 2004: Continuous observations of Asian dust and other aerosols by polarization lidars in China and Japan during ACE-Asia. *J. Geophys. Res*. **109**,

For Peer Review Only

doi:10.1029/2002JD003253.

Shin, S., Müller, D., Kim, Y. J., Tatarov, B., Shin, D., Seifert, P., and Noh, Y. M., 2013: The retrieval of the Asian dust depolarization ratio in Korea with the correction of the polarization-dependent transmission. *Asia-Pacific Journal of Atmospheric Sciences*, **49(1)**, 19-25.

Shin, S., Noh, Y. M., Lee, K., Lee, H., Müller, D., Kim, Y. J., Kim, K, and Shin, D., 2014: Retrieval of the single scattering albedo of Asian dust mixed with pollutants using lidar observations. *Advances in Atmospheric Sciences*, **31(6)**, 1417-1426.

Shin, S. K., Müller, D., Lee, K. H., Shin, D., Kim, Y. J., and Noh, Y. M., 2015: Vertical variation of optical properties of mixed Asian dust/pollution plumes according to pathway of airmass transport over East Asia. *Atmospheric Chemistry and Physics*, 15, 6707-6720.

Stocker, T.F., Qin, D., Plattner, G.-K., Tignor, M., Allen, S.K., Boschung, J., Nauels, A., Xia, Y., Bex, V., Midgley, P.M., 2013: IPCC, 2013: Climate Change 2013: The Physical Science Basis. Contribution of working group I to the fourth assessment report of the intergovernmental panel on climate change. *Cambridge University Press*, Cambridge, United Kingdom and New York, NY, USA.

Takemura, T., Nozawa, T., Emori, S., Nakajima, T. Y., & Nakajima, T., 2005: Simulation of climate response to aerosol direct and indirect effects with aerosol transport-radiation model. *J. Geophys. Res*., **110**, D02202, doi:10.1029/2004JD005029.

Tesche, M., Müller, D., Gross, S., Ansmann, A., Althausen, D., Freudenthaler, V., Weinzierl, B., Veira, A., and Petzold, A., 2011: Optical and microphysical properties of smoke over Cape

For Peer Review Only

Verde inferred from multiwavelength lidar measurements. *Tellus B*, **63(4)**, 677-694.

Utry, N., Ajtai, T., Filep, Á., Pintér, M. D., Hoffer, A., Bozoki, Z., and Szabó, G., 2013: Mass specific optical absorption coefficient of HULIS aerosol measured by a four-wavelength photoacoustic spectrometer at NIR, VIS and UV wavelengths, *Atmos. Environ.*, **69**,321–324.

Volten, H., Munoz, O., Rol, E., Haan, J. D., Vassen, W., Hovenier, J. W., Muinonen, K., and Nousiainen, T., 2001: Scattering matrices of mineral aerosol particles at 441.6 nm and 632.8 nm. *J. Geophys. Res.*, **106**, 17375–17401.

Yoon, S. C., Lee, Y. J., Kim, S. W., Kim, M. H., and Sugimoto, N., 2010: Measurements of the Lidar ratio for asian dust and pollution aerosols with a combined raman and back-scatter lidar. *Journal of the Korean Meteorological Society*, **20(4)**, 387-530.

For Peer Review Only

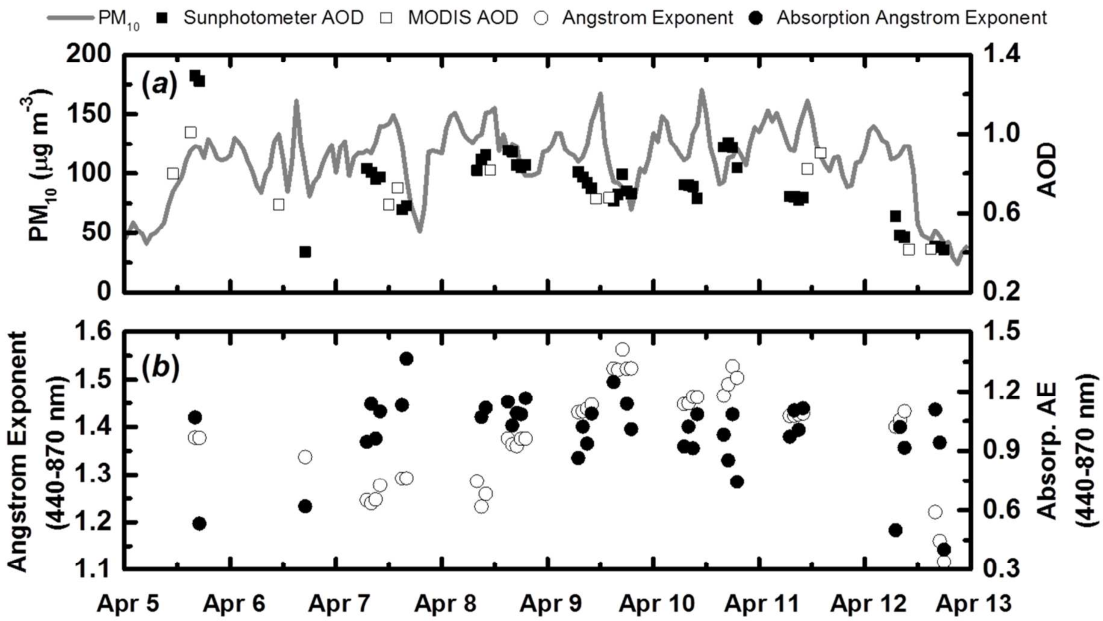

Fig. 1. (a) Time series of the PM_{10} concentration (gray line) measured with a beta gauge, the AERONET sun/sky radiometer AOD (black square) at 500 nm, and MODIS AOD (open square) at 550 nm (b) Ångström exponent and absorption Ångström exponent (440–870 nm wavelength range) derived from the AERONET sun/sky radiometer data.

For Review Only

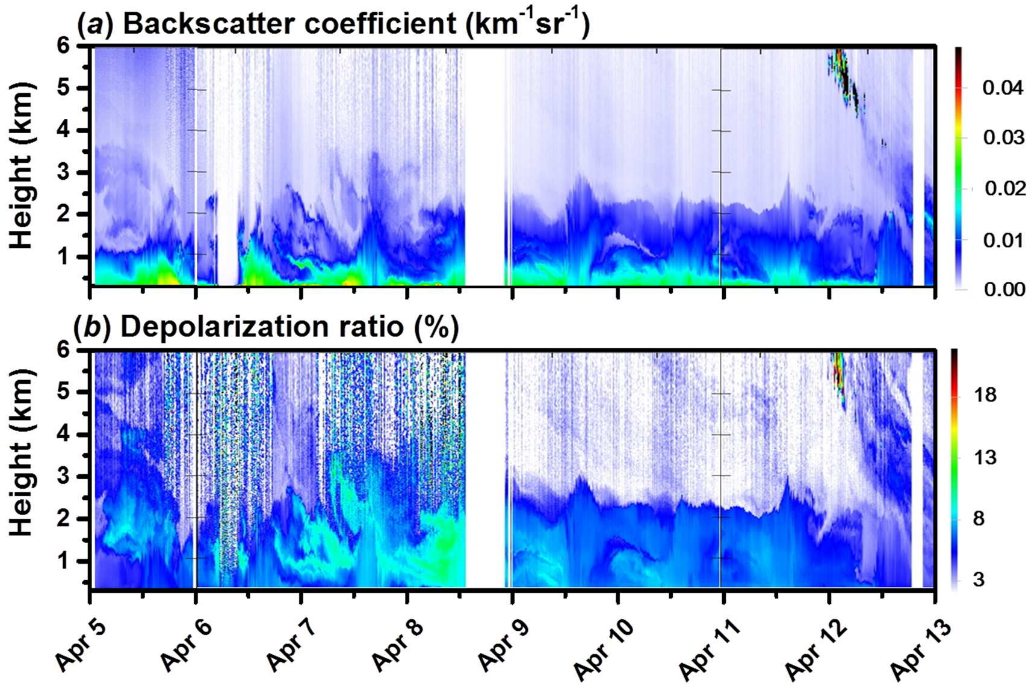

Fig. 2. Time–height cross-sections of (a) the 532 nm attenuated backscattered coefficient and (b) the linear volume depolarization ratios observed by the depolarization ratio lidar system between April 5 (00:00 LT) and 12 (24:00 LT) 2009.

Review Only

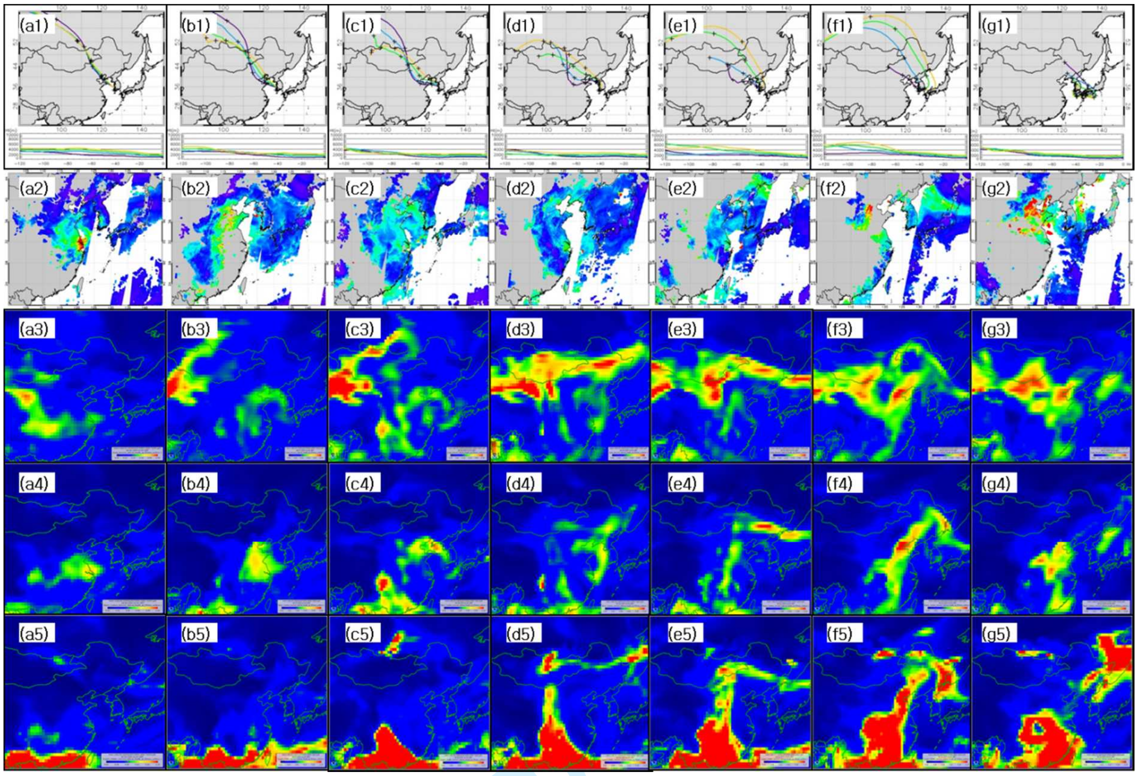

Fig. 3. Five-day HYSPLIT backward trajectory analysis (a1–g1), MODIS-derived aerosol optical depth at 550 nm (a2–g2), and the ECMWF-derived distributions of the aerosol optical depth for dust (a3–g3), black carbon (a4–g4), and organic matter (a5–g5) over East Asia for April 6 to 12 2009.

For Review Only

Fig. 4. MODIS active fire products for April 9–12 2009.

For Review Only

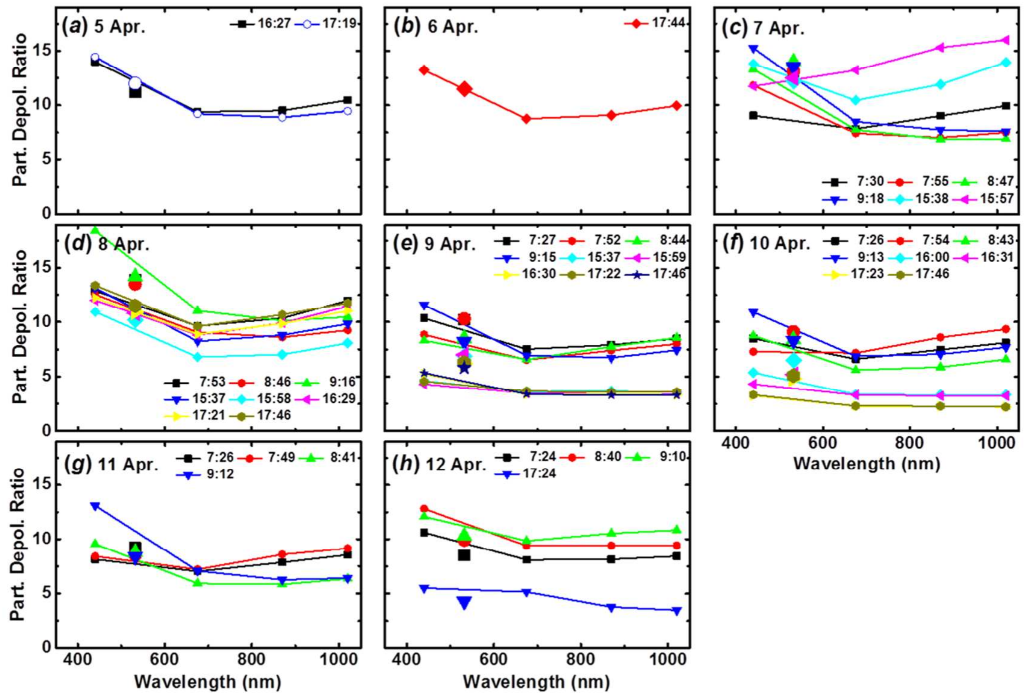

Fig. 5. Particle depolarization ratio at four wavelengths (440, 675, 870, and 1020 nm) derived from the AERONET sun/sky radiometer data (dotted lines) and lidar-derived depolarization ratio (large dots) at 532 nm. Lidar-derived DPRs are represented by dots, whereas the sun/sky radiometer-derived DPRs are represented by line with dot. Observation days and times are as in Fig. 2.

For Peer Review Only

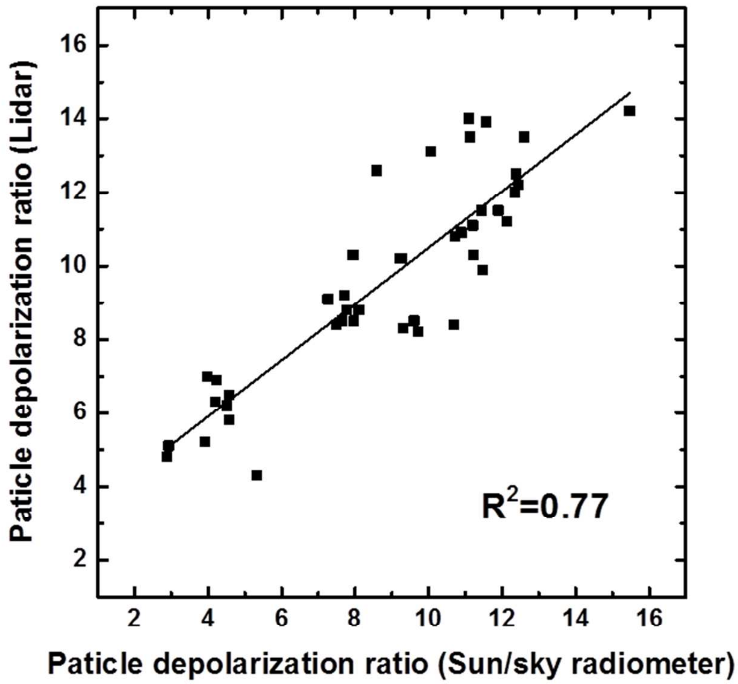

Fig. 6. Correlation plot of particle depolarization ratio at 532 nm derived by lidar and sun/sky radiometer data. The particle depolarization ratio of sun/sky radiometer at 532 nm was calculated by the linear regression method.

For Review Only

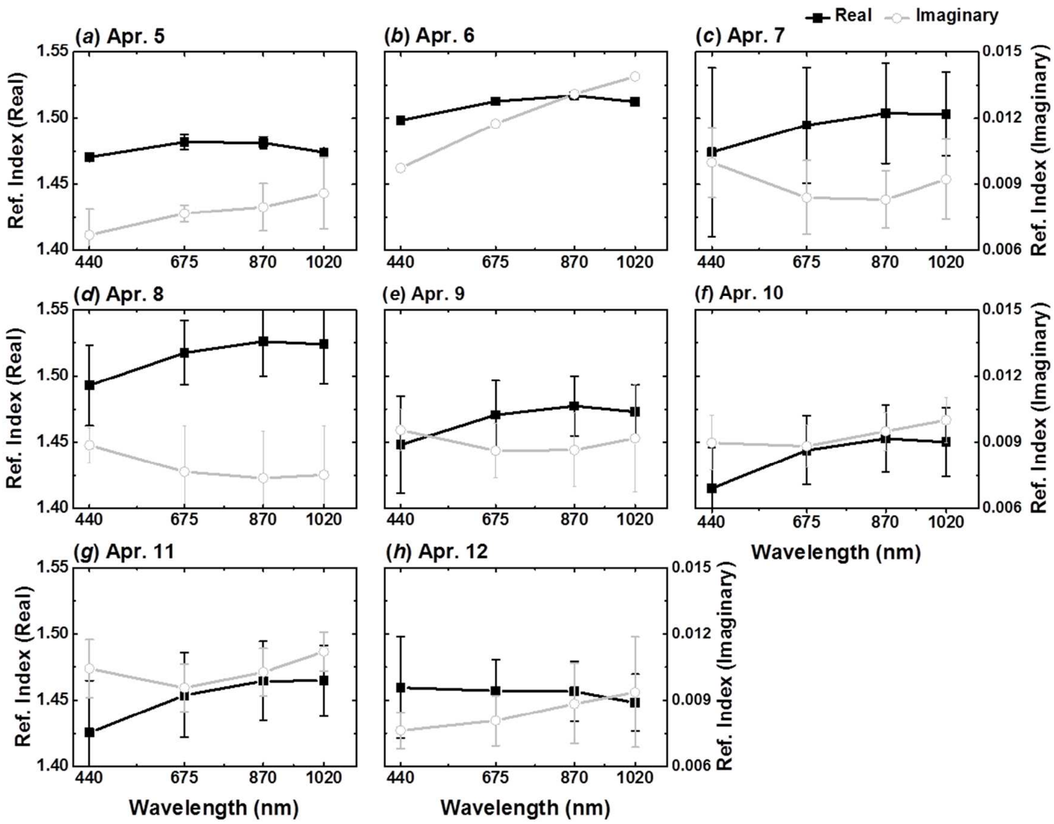

Fig. 7. Refractive index (real part (black squares) + imaginary part (open circles)) of particles with respect to the measured wavelengths (440, 675, 870, and 1020 nm), as retrieved from the AERONET sun/sky radiometer measurements on April 5 to 12 2009. The number of measurement data for each day is the same in Figure 5.

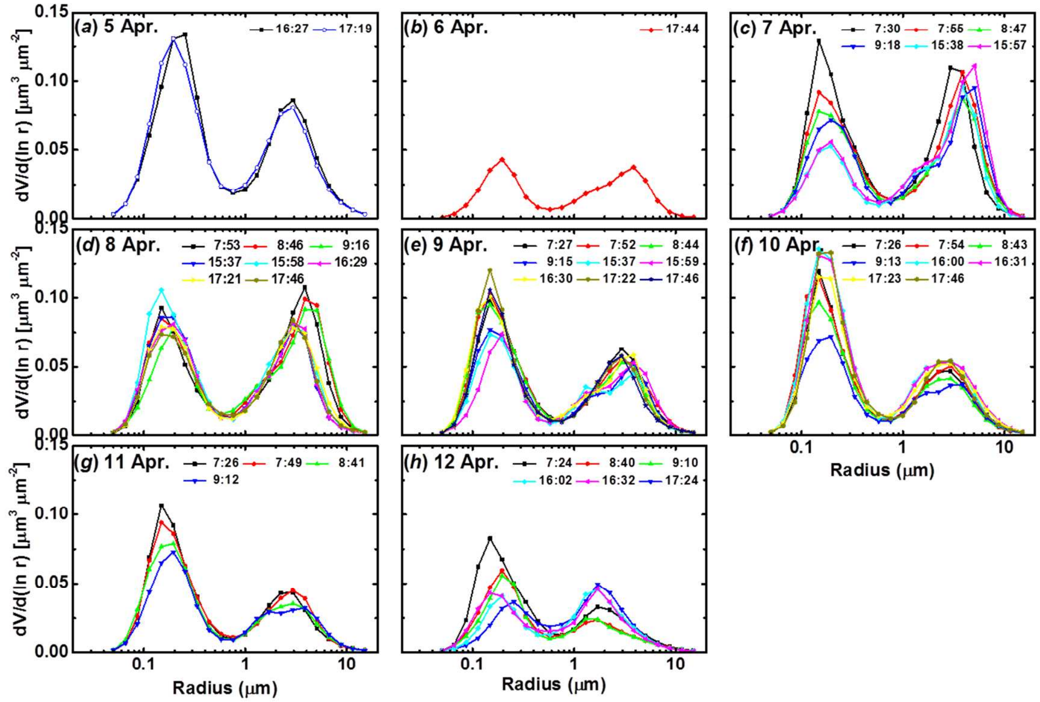

Fig. 8. Particle volume size distribution retrieved from the AERONET sun/sky radiometer on April 5 to 12 2009. Observation times are shown for each day.

Review Only

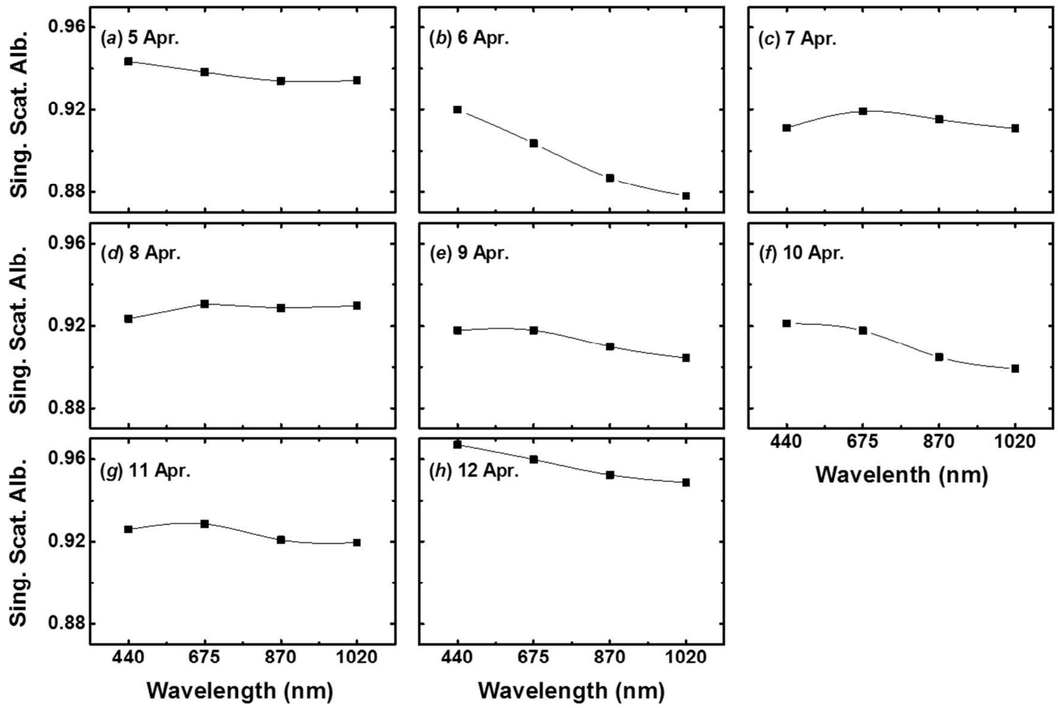

Fig. 9. Daily averaged spectral single scattering albedo at 440, 675, 870, and 1020 nm by AERONET Version 2, Level 2.0 data from April 5 to 12 2009.

Review Only

Table 1. Daily average values of aerosol optical depth (**τ**) at 500 nm, AE, sun/sky radiometer-derived particle depolarization ratios (**δ_{sp}**) at 440, 675, 870, and 1020 nm, and AAE.

Date	**τ** (500 nm)	AE (440-870nm)	**δ_{sp}** (%) 440 nm	675 nm	870 nm	1020 nm	AAE (440-870 nm)
5 Apr.	1.28 ± 0.02	1.38	14.2 ± 0.3	9.3 ± 0.1	9.2 ± 0.4	10.0 ± 0.7	0.80 ± 0.38
6 Apr.	0.40	1.34	13.2	8.8	9.1	10.0	0.62
7 Apr.	0.74 ± 0.09	1.27 ± 0.02	12.5 ± 2.1	9.2 ± 2.2	9.7 ± 3.3	10.3 ± 3.8	1.11 ± 0.15
8 Apr.	0.86 ± 0.04	1.33 ± 0.06	13.2 ± 2.2	9.0 ± 1.2	9.4 ± 1.2	10.5 ± 1.4	1.26 ± 0.46
9 Apr.	0.74 ± 0.05	1.49 ± 0.05	6.2 ± 3.5	5.0 ± 1.8	5.2 ± 2.1	5.5 ± 2.5	1.16 ± 0.26
10 Apr.	0.82 ± 0.11	1.48 ± 1.43	5.8 ± 3.4	4.7 ± 2.1	5.0 ± 2.5	5.3 ± 2.9	0.95 ± 0.12
11 Apr.	0.68 ± 0.01	1.43	9.8 ± 2.3	6.8 ± 0.6	7.1 ± 1.3	7.6 ± 1.4	1.05 ± 0.07
12 Apr.	0.47 ± 0.06	1.29 ± 0.14	12.0 ± 3.8	10.3 ± 4.2	10.3 ± 4.8	10.7 ± 5.2	0.81 ± 0.29

For Peer Review Only